Journal of Computational Physics **154,** 41–64 (1999)
Article ID jcph.1999.6297, available online at http://www.idealibrary.com on IDEAL®

Analysis of Stiffness in the Immersed Boundary Method and Implications for Time-Stepping Schemes

John M. Stockie* and Brian R. Wetton†

*Department of Mathematics and Statistics, Simon Fraser University, Burnaby, British Columbia, Canada, V5A 1S6; and †Department of Mathematics, University of British Columbia, Vancouver, British Columbia, Canada, V6T 1Z2

E-mail: *jms@sfu.ca and †wetton@math.ubc.ca

Received June 14, 1998; revised March 18, 1999

The immersed boundary method is known to exhibit a high degree of numerical stiffness associated with the interaction of immersed elastic fibres with the surrounding fluid. We perform a linear analysis of the underlying equations of motion for immersed fibres, and identify a discrete set of *fibre modes* which are associated solely with the presence of the fibre. This work generalises our results in a previous paper (1995, *SIAM J. Appl. Math.* **55**, 1577) by incorporating the effect of spreading the singular fibre force over a finite "smoothing radius," corresponding to the approximate delta function used in the immersed boundary method. We investigate the stability of the fibre modes, their stiffness, and their dependence on the problem parameters, focusing on the influence of smoothing. We then extend the analytical results to include the effect of time discretisation, and draw conclusions about the time step restrictions on various explicit schemes, as well as the convergence rates for an iterative, semi-implicit method. We draw comparisons with computations and show how the results can be applied to help in choosing alternate time-stepping schemes that are specially tailored to handle the stiffness in immersed fibres. In particular, we present numerical results that show how fully explicit Runge–Kutta schemes perform in comparison with the best of the semi-implicit schemes currently in use.

Key Words: immersed boundary method; linear stability; time-stepping schemes.

1. INTRODUCTION

Some of the most challenging problems in scientific computation involve the interaction of a viscous fluid with complex, moving boundaries. One approach that has proven particularly effective in handling a variety of such problems is the *Immersed Boundary Method*, which

0021-9991/99 $30.00

was originally developed by Peskin [15] to compute the flow of blood in a two-dimensional model of the heart. The method is a mixed Eulerian–Lagrangian scheme, in which the equations describing the fluid motion are discretised on a fixed, Cartesian mesh, while the immersed boundary is tracked at a set of points that move relative to the underlying fluid grid. The coupling between the fluid and fibre is accomplished using smoothed delta functions, which serve to interpolate quantities between the two grids. The method has since been extended to three-dimensional simulations of flow in the heart and arteries [20, 16] and a diverse collection of other problems, including swimming motions of marine worms [6], particle suspensions [8], and wood pulp fibre dynamics [22], to name a few. Furthermore, the idea of using smoothed delta functions to approximate singular forces generated on internal boundaries is a technique that has recently been applied in concert with a variety of other numerical methods including particle-in-cell [10], finite element [24, 26], and level set methods [3].

Considering the widespread use of immersed boundaries as a modeling and computational tool, very little analysis has been performed on either the underlying model equations or the numerical method. Exact solutions were derived for a fibre immersed in an inviscid fluid [5], and for variations of the problem specialised for viscous flow through particle suspensions [7] and in the inner ear [12]. Beyer and LeVeque [2] analysed a one-dimensional version of the immersed boundary method, and showed that it is limited to first order spatial accuracy by the delta function approximation. This limitation on accuracy has also been confirmed computationally in higher dimensions [11]. Computations also indicate that the problem suffers from a high level of numerical stiffness, and considerable effort has gone into developing semi-implicit variants of the method that aim to alleviate the severe time step restrictions [25, 13]. However, these attempts have met with limited success, and the majority of computations are still performed using an explicit treatment of the immersed boundary.

Our purpose in this paper is two-fold: first, to examine the stability and stiffness characteristics of incompressible, viscous fluid flows containing moving, elastic fibres; and second, to use these results as a basis for evaluating the efficiency of various explicit and semi-implicit time-stepping schemes. This work is based on an earlier paper [23] that employed a linear stability analysis to identify solution modes arising solely from the presence of an immersed fibre. The severe stiffness observed in computations was traced to the presence of these "fibre modes," and attributed to a combination of small viscosity and large fibre force. Hence, fluid flows with immersed fibres experience something very unlike the usual *Reynolds number limitation* encountered in flows without a fibre. While our previous paper was able to pinpoint the source of the stiffness and its dependence on the parameters, the predicted time step restrictions were much smaller than those actually experienced in computations.

In the current paper, we address this discrepancy by including the effects of smoothing through delta function approximation, and thereby gain a better quantitative measure of the stiffness inherent in fibre modes. We begin in Section 2 with a statement of the equations governing the motion of an isolated fibre immersed in a two-dimensional Stokes flow, and then briefly outline the immersed boundary method. The linear analysis of the immersed fibre problem with a smoothed forcing term is performed in Section 3, which yields a dispersion relation for the fibre modes. The behaviour of these modes is compared to computed solutions and to our earlier work on the analytical solution for the exact delta function problem. Section 4 extends our analysis to time discretisations, and uses stability diagrams to investigate the time step restrictions on schemes that are explicit in the fibre force. We explore a particular semi-implicit discretisation, which can be formulated as

an iteration on the fibre position, and verify the predicted convergence rates in numerical experiments. Finally, through comparisons of the various time-stepping schemes, we show that a fully explicit, fourth order Runge–Kutta method can be competitive with the semi-implicit schemes that are currently in use.

2. IMMERSED FIBRES

For the remainder of this work, we will consider an isolated fibre Γ, immersed within a rectangular domain Ω that is filled with a viscous, incompressible fluid (refer to Fig. 1). We single out a lone fibre for reasons of mathematical convenience, a simplification which seems reasonable when one considers that even the most complex immersed surfaces in three dimensions, such as the heart model in [16], are constructed of interwoven networks of such fibres. The fibre is assumed massless and neutrally buoyant, so that the fluid and fibre can be treated as a composite, viscoelastic material, described by a single velocity field. This is the major advantage of the model, since it allows the fluid and fibre to be described by the same set of equations.

2.1. *Mathematical Formulation*

Consider a square fluid domain, $\Omega = [0, 1] \times [0, 1]$, with periodic boundary conditions in both the x- and y-directions. The motion of the fluid–fibre composite is governed by Stokes' equations

$$\rho \frac{\partial \mathbf{u}}{\partial t} = \mu \Delta \mathbf{u} - \nabla p + \mathbf{F}, \tag{1}$$

$$\nabla \cdot \mathbf{u} = 0, \tag{2}$$

where $\mathbf{u}(\mathbf{x}, t) = (u(\mathbf{x}, t), v(\mathbf{x}, t))$ is the fluid velocity, $p(\mathbf{x}, t)$ is the pressure, $\mathbf{F}(\mathbf{x}, t)$ is the fluid body force, and ρ and μ are the (constant) fluid density and viscosity.

Our reason for considering Stokes' equations (and ignoring the effects of convection) is that the serious numerical stability problems encountered in computations are well known to arise from the stiffness in the immersed boundary. While high Reynolds number flows do require a finer mesh to resolve the boundary layer effects around complex elastic structures,

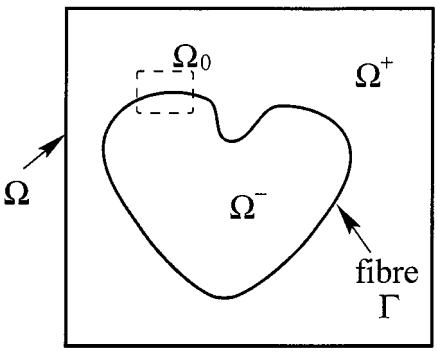

FIG. 1. The two-dimensional model: a fluid domain, Ω, which is divided into two parts, Ω^+ and Ω^-, by an immersed fibre Γ.

and thereby naturally require a smaller time step, there is no inherent Reynolds number limit on the immersed boundary method. The method is not tied to a specific fluid solver, and even when one uses alternate solvers specially tailored to handle convection-dominated flows, the stiffness in the immersed fibres is still the major consideration [19].

The position of the fibre is given by $\mathbf{x} = \mathbf{X}(s, t)$, where s is a parameterisation of Γ in some reference configuration. Since Γ is constrained to move at the same velocity as neighbouring fluid particles, we write

$$\frac{\partial \mathbf{X}}{\partial t} = \mathbf{u}(\mathbf{X}(s, t), t). \tag{3}$$

The final element needed to close the system is an expression for the force $\mathbf{F}$. Because the fibre is neutrally buoyant, we assume that gravitational effects are negligible, so that the external force $\mathbf{F}$ arises solely from the action of the elastic fibre. Let $T(s, t)$ be the tension force in the fibre and assume that T is a function of the fibre strain:

$$T = T\left(\left|\frac{\partial \mathbf{X}}{\partial s}\right|\right). \tag{4}$$

It can be shown under further assumptions [16] that the local force density per unit length is given by the expression

$$\mathbf{f}(s, t) = \frac{\partial}{\partial s}(T\boldsymbol{\tau}), \tag{5}$$

where $\boldsymbol{\tau}$ is the unit tangent vector to Γ. For example, if the tension depends linearly on the strain as $T = \sigma|\partial \mathbf{X}/\partial s|$, then Eq. (5) reduces to

$$\mathbf{f} = \sigma \frac{\partial^2 \mathbf{X}}{\partial s^2}. \tag{6}$$

Taking (6) as the force density is analogous to linking successive fibre points by linear springs with spring constant σ and zero resting length.

Since the force is zero everywhere except on the fibre, the fluid body force $\mathbf{F}$ can be regarded as a distribution and written compactly as the convolution of the fibre force density with a delta function,

$$\mathbf{F}(\mathbf{x}, t) = \int_\Gamma \mathbf{f}(s, t) \cdot \delta(\mathbf{x} - \mathbf{X}(s, t))\, ds, \tag{7}$$

where $\delta(\mathbf{x}) = \delta(x) \cdot \delta(y)$ is the product of two Dirac delta functions. Finally, we rewrite the right hand side of the fibre evolution equation (3) in the form of a convolution of the velocity with a delta function

$$\frac{\partial \mathbf{X}}{\partial t} = \int_\Omega \mathbf{u}(\mathbf{x}(s, t), t) \cdot \delta(\mathbf{x} - \mathbf{X}(s, t))\, d\mathbf{x}. \tag{8}$$

There is now clearly a certain symmetry between Eqs. (7) and (8), which will prove to be very useful in Section 2.2 from the standpoint of constructing a numerical scheme. Equations (1), (2), and (8), along with the definition of the fibre force in (4), (5), and (7), form a coupled system of integro-differential equations for the motion of the fluid and fibre.

It is important to mention that there is another, equivalent formulation of the problem, in which the singular delta function terms are supplanted by jump conditions that relate the fluid stress on either side of the fibre. This "jump formulation" was the basis of our analysis in [23], but is inappropriate for the current work where our aim is to determine the investigate the effect of replacing the delta function with a smooth approximation.

2.2. *Immersed Boundary Method*

There are many variants of the immersed boundary method, but we will present the method in a form very similar to that originally proposed in [15], and which is still commonly in use. This scheme is explicit in the fibre force, and any discussion of details related to semi-implicit discretisations will be postponed until Section 4 when they are needed.

The fluid domain is divided into a fixed, $N \times N$ grid of points denoted $\mathbf{x}_{i,j} = (x_i, y_j) = (ih, jh)$, with spacing $h = 1/N$ in both directions. The domain is doubly periodic so that the points x_0 and x_N are identified with each other, and similarly with y_0 and y_N. The fibre position is a Lagrangian quantity which is discretised at a set of N_b moving points, with the parameter $s \in [0, 1]$ taken at discrete locations $s_l = l \cdot h_b$, where $h_b = 1/N_b$. Both fluid and fibre unknowns are sampled at equally spaced time intervals $t_n = n \cdot k$, where k is the time step. Figure 2 shows a typical fluid–fibre grid. The discrete velocity is written as $u^n_{i,j} \approx \mathbf{u}(x_i, y_j, t_n)$ at fluid grid points $i, j = 0, 1, \ldots, N-1$ and $n = 0, 1, \ldots$, with analogous expressions for pressure and force. Similarly, the fibre position is denoted $\mathbf{X}^n_l \approx \mathbf{X}(s_l, t_n)$, for $l = 0, 1, \ldots, N_b - 1$.

The delta functions appearing in (7) and (8) are replaced by an approximation $\delta_{2h}(\mathbf{x})$, which is the product of two one-dimensional discrete delta functions

$$\delta_{2h}(x_i, y_j) = d_{2h}(x_i) \cdot d_{2h}(y_j).$$

The choice of d_{2h} most commonly used in immersed boundary computations is

$$d_{2h}(r) = \begin{cases} \frac{1}{4h}\left(1 + \cos\frac{\pi r}{2h}\right) & \text{if } |r| < 2h, \\ 0 & \text{if } |r| \geq 2h, \end{cases} \tag{9}$$

although other choices are possible [21]. It will become clear in the algorithm to follow that $\delta_{2h}(\mathbf{x})$ acts to interpolate quantities between the fluid and fibre grid points.

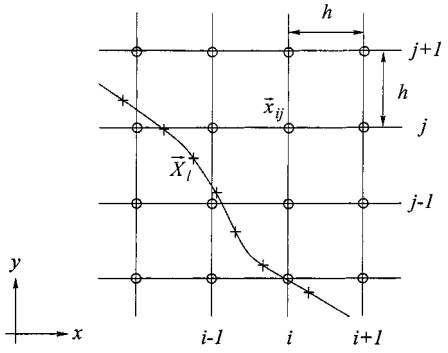

FIG. 2. The relationship between fluid (○) and fibre (+) grid points.

When writing the scheme, we will make use of the following notation for finite difference operators on the fluid grid. First and second derivatives are approximated using second order centered differences

$$D_x\phi_{i,j} = \frac{\phi_{i+1,j} - \phi_{i-1,j}}{2h} \qquad \text{and} \qquad D_{xx}\phi_{i,j} = \frac{\phi_{i+1,j} - 2\phi_{i,j} + \phi_{i-1,j}}{h^2},$$

with similar expressions for the y-derivatives, D_y and D_{yy}. The discrete gradient and Laplacian operators are then given by

$$\nabla_h\phi_{i,j} = (D_x,\ D_y)\,\phi_{i,j} \qquad \text{and} \qquad \Delta_h\phi_{i,j} = (D_{xx} + D_{yy})\,\phi_{i,j},$$

and the second derivative of fibre quantities is denoted $D_{ss}\psi_l$.

We are now in a position to state the algorithm, which is a discrete version of Eqs. (1), (2), (6), and (8). Assuming that the velocity $\mathbf{u}^n_{i,j}$ and fibre position $\mathbf{X}^n_{i,j}$ are known at time t_{n-1}, the procedure for updating these values to time t_n is as follows:

Step 1. Compute the fibre force density

$$\mathbf{f}^n_l = \sigma D_{ss}\mathbf{X}^{n-1}_l, \tag{10a}$$

where we have assumed, for simplicity, that the force is a linear function such as that in Eq. (6).

Step 2. Distribute the fibre force to fluid grid points

$$\mathbf{F}^n_{i,j} = \sum_{l=0}^{N_b-1} \mathbf{f}^n_l \cdot \delta_{2h}\left(\mathbf{x}_{i,j} - \mathbf{X}^{n-1}_{i,j}\right) \cdot h_b. \tag{10b}$$

Step 3. Solve the discrete Stokes problem

$$\rho\left(\frac{\mathbf{u}^n_{i,j} - \mathbf{u}^{n-1}_{i,j}}{k}\right) = \mu\Delta_h\mathbf{u}^n_{i,j} - \nabla_h p^n_{i,j} + \mathbf{F}^n_{i,j}, \tag{10c}$$

$$\nabla_h \cdot \mathbf{u}^n_{i,j} = 0, \tag{10d}$$

which is a simultaneous system of equations for the velocity $\mathbf{u}^n_{i,j}$ and pressure $p^n_{i,j}$ at time level n. Because the fluid grid is rectangular and equally spaced and the boundary conditions are periodic, this system can be solved very efficiently using a Fast Fourier Transform (see [14] for details).

Step 4. Evolve the fibre at the new local fluid velocity

$$\frac{\mathbf{X}^n_l - \mathbf{X}^{n-1}_l}{k} = \sum_{i,j=0}^{N-1} \mathbf{u}^n_{i,j} \cdot \delta_{2h}\left(\mathbf{x}_{i,j} - \mathbf{X}^{n-1}_l\right) \cdot h^2. \tag{10e}$$

Step 5. Increment n and return to Step 1.

Since this algorithm applies an implicit (Backward Euler) discretisation to diffusion terms, and a Forward Euler step for the fibre force and position, we will refer to it as the *Forward Euler/Backward Euler*, or *FE/BE*, method. This designation will also serve to distinguish it from other semi-implicit time-stepping schemes that will be introduced later, in Section 4.

3. LINEAR STABILITY ANALYSIS

As mentioned in the Introduction, a great deal of effort has gone into applying the immersed boundary method to various physical problems and improving its efficiency. However, comparatively little work has been done on analysing the behaviour of solutions to the underlying equations of motion [12, 7, 5]. In this section we will use an approach akin to that in [12, 7] to perform a *linear modal analysis* of the immersed fibre problem in a more general form. We are able to obtain details about discrete modes associated with immersed fibres which relate to the stiffness observed in immersed boundary computations.

3.1. *Linearisation and Smoothing*

Consider a portion of the fluid domain, labeled Ω_0 in Fig. 1, on which the immersed fibre is approximately flat. Suppose that the fibre is at equilibrium along the horizontal line $y = 0$, and that its current position is a small perturbation from this rest state. For the purpose of isolating the influence of the fibre on the flow, we extend the boundaries of Ω_0 to infinity in the y-direction as in [23].

A common form of the tension used in immersed boundary computations [25] is $T = T(|\partial \mathbf{X}/\partial s| - 1)$ with $T(0) = 0$, corresponding to a fibre which is slack in the reference configuration $|\partial \mathbf{X}/\partial s| = 1$. However, most physical applications involve fibres under tension, and so we choose an equilibrium state defined by $|\partial \mathbf{X}/\partial s| = \theta$, corresponding to a fibre that is either under tension ($\theta > 1$) or slack ($\theta = 1$) in its rest state. The solution is then linearised by supposing a perturbation of the form

$$\mathbf{X}(s, t) = (\theta s + \xi(s, t),\ \eta(s, t)), \tag{11}$$

and assuming that ξ, η, $\mathbf{u}$ and their derivatives are small.

We next incorporate the effect of smoothing the delta function which is inherent in the immersed boundary method. To this end, we introduce a strip of width ϵ, called the *smoothing region*, on either side of the fibre, where ϵ represents the radius of support of the approximate delta function. The fluid domain, Ω_0, is now divided into three subregions, Ω_0^+, Ω_0^-, and Ω_0^ϵ, as pictured in Fig. 3. The smoothed delta function, denoted $d_\epsilon(x)$, is the cosine function introduced in Eq. (9) with $\epsilon = 2h$ corresponding to the smoothing radius $\epsilon = 2h$ used in actual computations.

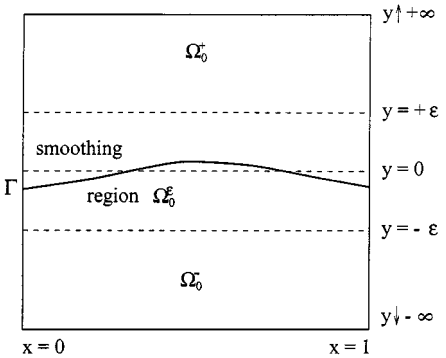

FIG. 3. A blow-up of the region Ω_0 in Fig. 1, with the fibre at equilibrium along $y = 0$, and the smoothing region Ω_0^ϵ, of width 2ϵ.

Stokes' equations now read

$$\rho \frac{\partial \mathbf{u}}{\partial t} = \mu \Delta \mathbf{u} - \nabla p + \int_\Gamma \mathbf{f}(s,t) \cdot \delta_\epsilon (\mathbf{x} - \mathbf{X}(s,t))\, ds, \tag{12}$$

$$\nabla \cdot \mathbf{u} = 0, \tag{13}$$

where the integral term has support only on the smoothing region Ω_0^ϵ, and is zero elsewhere. The linearisation of Eqs. (4) and (5) follows that of [23], and so we will simply state the result, that

$$\mathbf{f}(s,t) \approx \left(\sigma_t \frac{\partial^2 \xi}{\partial s^2},\ \sigma_n \frac{\partial^2 \eta}{\partial s^2} \right), \tag{14}$$

where the normal and tangential force coefficients are given by $\sigma_n := T(\theta)/\theta$ and $\sigma_t := T'(\theta)$. Finally, the fibre evolution equation can be written as an integral solely over the smoothing region:

$$\frac{\partial \mathbf{X}}{\partial t} = \int_{\Omega_0^\epsilon} \mathbf{u}(\mathbf{x},t) \cdot \delta_\epsilon (\mathbf{x} - \mathbf{X}(s,t))\, d\mathbf{x}. \tag{15}$$

The remainder of Section 3 is devoted to solving the linearised equations of motion and examining the behaviour of the resulting solution modes.

3.2. *Derivation of the Dispersion Relation*

We now look for separable solutions of Eqs. (12)–(15) that have the form of Fourier modes

$$\begin{Bmatrix} u \\ v \\ p \end{Bmatrix} = e^{\lambda t + \hat{\imath}\alpha x} \begin{Bmatrix} \hat{u}(y) \\ \hat{v}(y) \\ \hat{p}(y) \end{Bmatrix} \qquad \text{and} \qquad \begin{Bmatrix} \xi \\ \eta \end{Bmatrix} = e^{\lambda t + \hat{\imath}\alpha\theta s} \begin{Bmatrix} \hat{\xi} \\ \hat{\eta} \end{Bmatrix},$$

where the wavenumber α is a positive real number, and $\hat{\imath} = \sqrt{-1}$ is the imaginary unit. The *exponential time factor* λ embodies the growth or decay characteristics of each solution mode. One such solution must be found for u, v, and p on each of the three subdomains $\Omega_0^\pm$ and Ω_0^ϵ. After these expressions are substituted into Eqs. (12) and (13) on $\Omega_0^\pm$, where the force term is zero, Stokes' equations reduce to a system of ODEs with solution

$$\hat{p}^\pm(y) = A^\pm e^{\mp \alpha y}, \tag{16a}$$

$$\hat{u}^\pm(y) = B^\pm e^{\mp \beta y} - \frac{\hat{\imath}\alpha}{\rho\lambda} A^\pm e^{\mp \alpha y}, \tag{16b}$$

$$\hat{v}^\pm(y) = \pm \frac{\hat{\imath}\alpha}{\beta} B^\pm e^{\mp \beta y} \pm \frac{\alpha}{\rho\lambda} A^\pm e^{\mp \alpha y}, \tag{16c}$$

where β is a new parameter defined by $\beta^2 = \alpha^2 + \frac{\rho}{\mu}\lambda$ with $Re(\beta) \geq 0$.

Within the smoothing region, the integral forcing terms lead to a system of coupled integro-differential equations. After we linearise the delta functions and drop all terms of

second order or higher in the "ˆ" solution components, these equations reduce to [21]

$$\left(\rho\lambda + \mu\alpha^2 - \mu\frac{d^2}{dy^2}\right)\hat{u}^\epsilon + \hat{\imath}\alpha\,\hat{p}^\epsilon = -\sigma_t\theta\alpha^2\hat{D}_\epsilon\hat{\xi}\,d_\epsilon(y), \tag{17a}$$

$$\left(\rho\lambda + \mu\alpha^2 - \mu\frac{d^2}{dy^2}\right)\hat{v}^\epsilon + \frac{d\hat{p}^\epsilon}{dy} = -\sigma_n\theta\alpha^2\hat{D}_\epsilon\hat{\eta}\,d_\epsilon(y), \tag{17b}$$

$$\hat{\imath}\alpha\hat{u}^\epsilon + \frac{d\hat{v}^\epsilon}{dy} = 0, \tag{17c}$$

$$\lambda\hat{\xi} = \hat{D}_\epsilon\int_{-\epsilon}^{\epsilon}\hat{u}^\epsilon(y)\cdot d_\epsilon(y)\,dy, \tag{17d}$$

$$\lambda\hat{\eta} = \hat{D}_\epsilon\int_{-\epsilon}^{\epsilon}\hat{v}^\epsilon(y)\cdot d_\epsilon(y)\,dy. \tag{17e}$$

The expression $\hat{D}_\epsilon$ arising above is the Fourier transform of the smoothed delta function, which for the cosine approximation is

$$\hat{D}_\epsilon := \int_{-\epsilon}^{\epsilon} e^{\hat{\imath}\alpha r}d_\epsilon(r)\,dr = \frac{\pi^2\sin(\alpha\epsilon)}{\alpha\epsilon\,(\pi^2-\alpha^2\epsilon^2)}.$$

We draw the reader's attention to the fact that the parameter θ, distinguishing slack fibres from those under tension, appears simply as a multiple of the forcing parameter in (17a) and (17b). Consequently, we will assume for the remainder that $\theta \equiv 1$, which is equivalent to a rescaling of σ_n and σ_t. We should mention that Cortez and Varela's analysis of a circular fibre [5] identifies a significant difference between the motion of a fibre depending on whether it is slack or under tension. However, their results are restricted to inviscid flow, and apply to the bulk motion (wavenumber $\alpha = 0$) of the fibre. Our "flat fibre" analysis, on the other hand, is insensitive to vertical translations of the fibre and is intended instead to capture the behaviour of the wavenumbers $\alpha > 0$.

Since $\hat{\xi}$ and $\hat{\eta}$ are constants, one may solve (17a)–(17c) for the velocity and pressure without knowing the fibre positions *a priori*. The resulting $\hat{u}^\epsilon$ and $\hat{v}^\epsilon$ are substituted into (17d) and (17e), yielding expressions for $\hat{\xi}$ and $\hat{\eta}$, which are then used to find the velocity. This procedure involves extensive algebraic manipulations, for which we found the symbolic algebra package MAPLE [4] indispensable. Unlike the solutions (16a)–(16c) on $\Omega_0^\pm$, the expressions on Ω_0^ϵ are extremely lengthy, and so they are not presented here.

At this point, we have expressions for the solution components on three regions, each involving several unknown constants of integration. On $\Omega_0^\pm$, Eqs. (16a)–(16c) involve the four coefficients $A^\pm$ and $B^\pm$, and the solution on Ω_0^ϵ introduces an additional four constants of integration. In order to determine the solution uniquely, we require a further eight conditions relating the eight constants, which arise quite naturally from matching the solutions at the interfaces $y = \pm\epsilon$. Four matching conditions ensue from the requirement that the pressure, velocities, and normal derivative $d\hat{u}/dy$ be continuous at the interface $y = \epsilon$, and the remaining constraints arise from continuity at $y = -\epsilon$.

The resulting system of equations is linear and homogeneous, and so there is a non-trivial solution only if the determinant of the 8×8 coefficient matrix is zero. The determinant condition is simply a *dispersion relation*, whose solutions give λ as functions of α. The dispersion relation is fairly complicated, and so is presented separately in the Appendix,

although it can be written symbolically as

$$S_n^\epsilon(\beta) \cdot S_t^\epsilon(\beta) = 0. \tag{18}$$

The subscripts n and t on the two factors in (18) correspond to the fact that the fibre force parameter σ_n appears only in the factor $S_n^\epsilon(\beta)$, while $S_t^\epsilon(\beta)$ depends only on σ_t. After (18) is solved for roots β, the growth rates are obtained via $\lambda = \frac{\mu}{\rho}(\beta^2 - \alpha^2)$.

As in the dispersion relation for the unsmoothed problem from [23], there is a decoupling between the normal and tangential fibre modes. However, the dispersion relation is no longer a polynomial, as it was for the jump problem, since the factors in Eq. (18) involve trigonometric and exponential functions of the parameters (see the Appendix). Consequently, there is no analytical expression for the solutions β and our only recourse is to apply a numerical root-finding technique such as Newton's method. The presence of exponential terms in the dispersion relation makes the equation very ill-conditioned, particularly when the wavenumber or the force is large. The Newton solver requires a careful rescaling of the dispersion relation in conjunction with quadruple precision arithmetic and continuation in ϵ.

3.3. *Stability and Stiffness of Fibre Modes*

In order to make these results as applicable as possible to previous work, we have chosen representative parameter values from computations reported in the literature for biological applications (primarily from [6, 15, 16]). We choose $\rho = 1.0\ \mathrm{g/cm^3}$ and the forcing parameter σ to lie between 10^4 and $10^6\ \mathrm{g/cm \cdot s^2}$, where $\sigma \equiv \sigma_n = \sigma_t$. The viscosity used in many biological applications (involving intra-cellular fluid, for example) is $\mu = 0.01\ \mathrm{g/cm \cdot s}$, while that for blood is $0.04\ \mathrm{g/cm \cdot s}$. However, most immersed boundary simulations of the heart and arteries have been forced to take $\mu = 1.0$ in order to avoid limitations on the time step. The domain is a square with sides of length 1 cm, on which is laid a 64×64 computational grid, and the fibre is discretised at 196 points; i.e., $N = 64$, $\epsilon = \frac{2}{64}$, and $N_b = 196$. We performed grid refinement studies which demonstrate that the results we present next do not change significantly as the number of grid points is increased.

We now consider a discrete set of wavenumbers, $\alpha = 2\pi \cdot i$, for $i \in \{1, 2, \ldots, N\}$, corresponding to the modes that can be resolved on an equally spaced grid with mesh spacing $h = \frac{1}{N}$ in the x-direction. By restricting α in this manner, we are still dealing with the continuous equations but have discretised the problem *in an idealised sense*. We also choose the smoothing length $\epsilon = \frac{2}{N}$ to agree with the radius of support for the delta function in the immersed boundary method.

Stability. For all wavenumbers and parameter ranges that we have considered, the solution modes arising from the dispersion relation exhibit a decay rate with negative real part; that is, $Re(\lambda) < 0$. While this is not as strong a result as the stability proof presented in [21] for the jump formulation of the problem, it still provides compelling evidence that the smoothed fibre modes are also stable in time.

Stiffness. The stiffness of the immersed fibre problem is characterised by the size of the complex eigenvalues λ. A large variation in the magnitude of the real part $Re(\lambda)$ indicates a solution with components that decay on widely varying time scales; correspondingly, a large variation in $Im(\lambda)$ points to modes with disparate frequencies of oscillation. In both cases, the problem is distinguished by a mixture of time scales that differ in size by orders of magnitude: any computation based on such a problem requires the use of stiff solvers.

TABLE I
Comparison of the Maximum λ for Solution Modes of Stokes' Equations, the Jump Formulation, and the Smoothed Problem with $\sigma = 10^5$

	$\mu = 0.04$		$\mu = 1.0$	
	$\max \lvert Re(\lambda)\rvert$	$\max \lvert Im(\lambda)\rvert$	$\max \lvert Re(\lambda)\rvert$	$\max \lvert Im(\lambda)\rvert$
Stokes modes	6.4×10^3	0.0	1.6×10^5	0.0
Fibre modes (jump)	5.7×10^6	9.6×10^6	6.3×10^5	9.0×10^5
Fibre modes (smooth)	3.5×10^3	6.1×10^4	5.9×10^4	1.3×10^4

By examining the decay rates $Re(\lambda)$, and frequencies of oscillation $Im(\lambda)$, we can quantify the stiffness of the solution and its dependence on parameters. Table I summarizes the maximum values of λ for the jump and smoothed formulations of the problem, with $\sigma = 10^5$ representative of the range of forcing parameters encountered in physical problems. The *Stokes modes* correspond to solutions of Stokes' equations without an immersed fibre, for which $\lambda^S = -\frac{\mu}{\rho}\alpha^2$.

Let us begin by comparing the Stokes problem without a fibre to the "jump" problem with a delta function force, from which it is clear that the presence of an immersed fibre affects the rate of decay of solution modes considerably, while also introducing significant oscillatory features in the solution. The fibre therefore introduces a certain degree of stiffness in the problem, which translates numerically into a stricter requirement on the time step in the immersed boundary method. The magnitude of λ increases by a factor of 7 when $\mu = 1.0$, and by almost 2000 for $\mu = 0.04$. It is here that the unsmoothed analysis over-predicts the stiffness observed in computations. The maximum allowable time step typically depends inversely on the magnitude of the solution modes λ, from which the first two rows of Table I suggest that immersed boundary computations should require a time step orders of magnitude smaller than that for Stokes flow without a fibre. On the contrary, immersed boundary computations with the moderate forcing of $\sigma = 10^4$ exhibit time step restrictions comparable to those in flows without an immersed fibre, even when viscosity is taken as small as 0.04.

This discrepancy can be attributed to exclusion of smoothing effects in the jump formulation of the problem. The final row of Table I indicates that the smoothed modes are more comparable in size with the Stokes modes, and hence much more in line with what is seen in actual computations for this example. Nevertheless, the appearance of a large imaginary part of λ translates into a considerable degree of stiffness, which is also observed in computations for this parameter range. It is clear that it is necessary to include smoothing effects, as done in this paper, to predict time step restrictions for immersed boundary calculations.

Figure 4 gives a pictorial representation of the effect of smoothing on the entire discrete spectrum of fibre modes. Replacing the delta function with a smoothed approximation clearly has a profound effect on the decay and frequency characteristics of an immersed fibre, particularly for the larger wavenumbers. However, it appears that the lowest wavenumber modes (with $\alpha = 2\pi$) match quite well between the two problems, which suggests that the dominant solution features are relatively unchanged by smoothing.

It is interesting to compare the sizes of solution modes in terms of viscosity in Table I. While a reduction in μ decreases the stiffness of the Stokes problem considerably, the smoothed fibre modes are affected to a much lesser degree, with the modes only decreasing

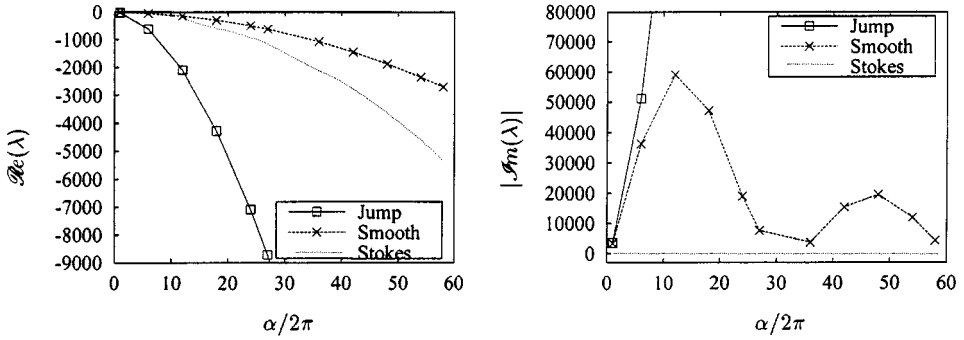

FIG. 4. A comparison of $Re(\lambda)$ and $Im(\lambda)$ for the jump and smoothed dispersion relations with $\alpha \in [2\pi, 128\pi]$, $\mu = 0.04$, and $\sigma = 10^5$.

by a factor of 2 in magnitude, and the imaginary part actually becoming larger (the implications of this behaviour for time-stepping will become obvious in the next section). On the other hand, the dependence of the fibre modes on σ is much stronger, with the stiffness of the problem intensifying as the forcing parameter is increased. The σ dependence was not included in Table I, since a detailed discussion of the effect of σ and μ on the time step restrictions, along with comparisons to actual computations, will be given in Section 4.

Finally, we observed that without exception the largest growth rates arose from the *tangential* term in dispersion relation, with the normal modes smaller and similar in magnitude to Stokes' modes. This is consistent with the asymptotic result of our previous work which showed that the normal fibre modes are similar in magnitude to Stokes' modes in the large σ limit [23]. Therefore, the stiffness in the problem may be traced to tangential oscillations of the immersed fibre. It is very possible that the decoupling of the fibre modes may be exploited to develop more efficient numerical solvers, perhaps using some form of rescaling or preconditioning based on a local linearisation near the fibre which singles out the tangential motions.

4. TIME-STEPPING SCHEMES

The linear analysis of the preceding section showed that the fibre modes capture the qualitative behaviour manifested in computations, provided the smoothing effect of the delta function approximation is taken into account. We will now use these stiff fibre modes to explain the severe time step restriction on immersed boundary computations in which the fibre is treated explicitly. By *explicit* we refer to a method (such as the *FE/BE* approach outlined in Section 2.2) that treats the fibre position and forcing term explicitly, regardless of whether the viscous and pressure terms are treated implicitly or explicitly. As we will see in Section 4.1, it is in fact the fibre forcing terms that govern the time step in explicit computations.

The severe stiffness arising from the immersed boundary problem and the correspondingly strict time step limit in computations have been well documented in the literature [15, 25]. As a result, the importance of dealing with the immersed fibres in an implicit fashion is obvious, and a great deal of effort has gone into developing variations of the method that couple the fibre terms in the equations implicitly with the fluid. We have separated the various methods into the following four classes, based on the manner in which the fibre force term and fibre evolution equation are discretised:

A. *Explicit:* schemes that are explicit in the fibre force and position, and yet couple the diffusion terms implicitly (that include the *FE/BE* scheme of Section 2.2). The vast majority of recent computations couple diffusion and convection implicitly by combining an ADI step with a pressure projection step. More recently, it has been recognised that convection is not so important in relation to the stiffness arising from the fibre, and the fluid equations have been solved using a coupled Stokes solver, while treating convection terms explicitly using upwind differencing [17, 14].

B. "*Approximate implicit*"*:* a scheme that couples the fibre force with the fibre evolution equation to form an iteration on the fibre position that is independent of the fluid unknowns [15]. Once the iteration has converged, the *intermediate or predicted fibre position* is used to compute the fibre force in the fluid equations, which are then solved using the same techniques as those for the explicit schemes. While this is not truly an implicit scheme (and hence the name), the iteration helps to prevent violent instabilities in fibres with extremely large force parameters. An alternate formulation of this class of iterative schemes was developed in [8] in terms of minimising an energy functional for the fibre position.

C. *Semi-implicit:* schemes that couple the fibre with the fluid unknowns in an iterative fashion, such as the method proposed by Mayo and Peskin [13].

D. *Fully implicit:* schemes in which the fibre and fluid unknowns are solved simultaneously. Tu and Peskin [25] implemented a fully implicit solver for Stokes flow and showed that while it appeared to be unconditionally stable, this approach was far too expensive for practical computations.

It is methods A and B that have been used most often in practice, with the majority of recent computations using the explicit technique A. While the approximate implicit scheme does help to ease the severe stability restrictions in problems with extremely large σ, it is our experience that the added cost of the iteration embedded in each time step essentially wipes out any advantage that would have been gained by taking larger time steps. The predominance of explicit schemes, which are extremely simple to program, is thus not surprising.

Nonetheless, the stability restrictions on explicit computations persist, and remain a serious limitation on the type of problem that can be simulated numerically. We have shown that the stiffness arises not from Reynolds number effects, but rather from a large fibre forcing parameter. While implementing a better fluid solver might provide improved resolution of the fine-scale boundary layer effects present in high Reynolds number (convection-dominated) flows, it will not help deal with the stiffness in immersed boundary computations arising from the fibre forcing terms, which is present even in the absence of convection. On the contrary, it is essential that more efficient implicit or semi-implicit schemes be developed which deal specifically with the stiffness that dominates computations when the fibre forcing term is large.

In this section, we restrict our attention to explicit and semi-implicit schemes. The fibre modes derived in the last section will be used to derive stability restrictions for various explicit time-stepping schemes, using a straightforward application of stability diagrams. The Runge–Kutta family of schemes exhibits the most desirable properties of explicit schemes, and we briefly describe a class of semi-implicit schemes, similar to the *FE/BE* method, but which use an Implicit–Explicit Runge–Kutta (or *IMEX–RK*) approach instead. Finally, we demonstrate how our modal analysis can be extended to time discrete problems, and this

technique will be applied to the Mayo–Peskin method in order to estimate convergence rates for the iteration.

4.1. *Explicit Schemes*

In the following discussion, we distinguish between the solution modes arising from an idealised discretisation of the smoothed fibre, and those from Stokes flow without an immersed boundary, since the time step in a discretisation of the immersed fibre problem is limited by a combination of diffusive and fibre effects. Figure 5 depicts the relative size of both sets of solution modes in the λ-plane, for $\sigma = 10^4$ and 10^6, with the Stokes modes

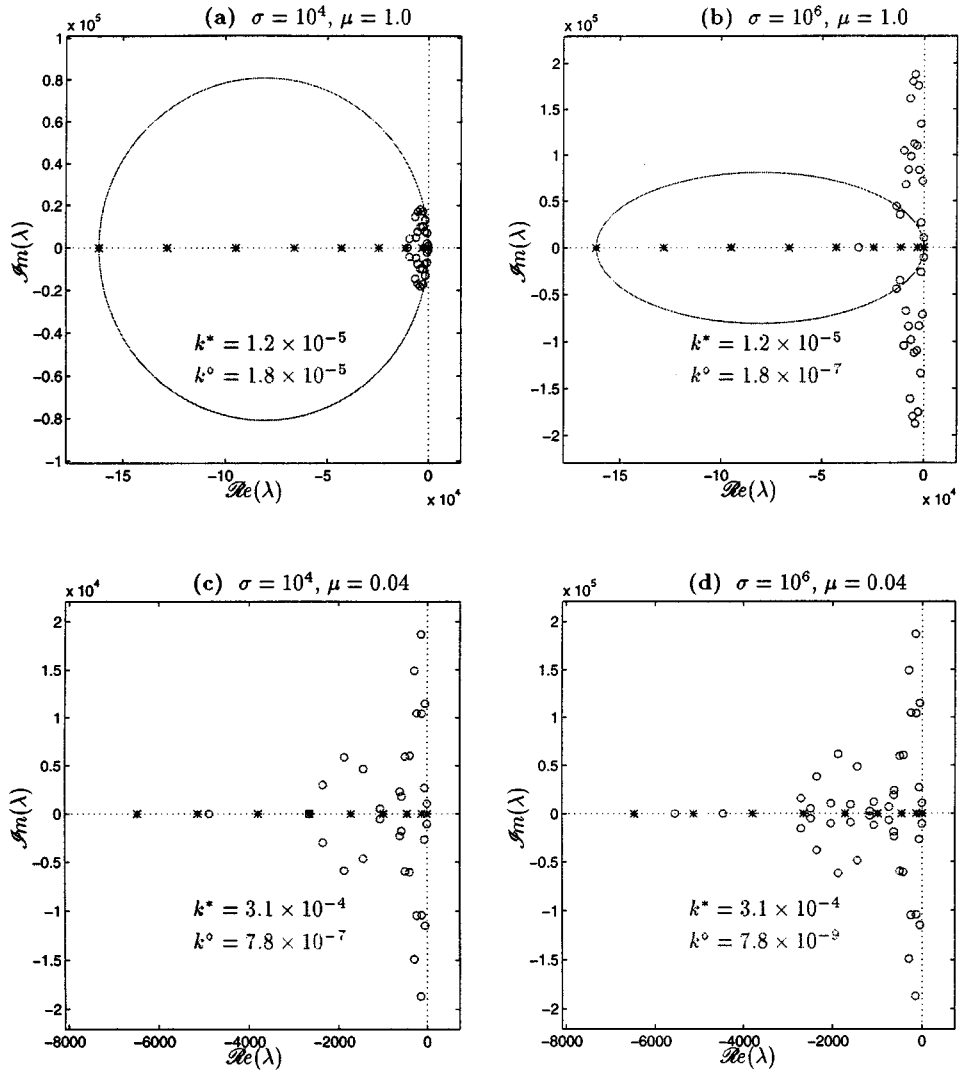

FIG. 5. Region of absolute stability for the Forward Euler scheme, along with the smoothed fibre modes (○) from Eq. (18), and Stokes modes (∗) from $\lambda = -\frac{\mu}{\rho}\alpha^2$. The stability boundary, drawn as a solid line in plots (a) and (b), is computed on the basis of the Stokes modes, while the maximum allowable time steps, k^* and k°, are listed for each set of modes. Note the difference in the scales used on the vertical axes, particularly from (a) → (b), and (c) → (d).

marked $*$ and fibre modes $\circ$. Note that these plots correspond to the complete set of modes for the results presented earlier in Table I. The solid curves represent the boundary of the region of absolute stability for a Forward Euler discretisation, based on Stokes modes, while the maximum time step allowed by Forward Euler for both sets of modes (denoted k^* and k°) are listed on each plot for easy comparison of the stability limits. Figure 5(a), corresponding to $\mu = 1.0$, demonstrates that the time step restriction for a fibre force of $\sigma = 10^4$ is comparable to that experienced in the absence of the fibre. When σ is increased to 10^6 in Fig. 5(b), however, the modes migrate outward along the imaginary axis, requiring a much smaller time step. A similar worsening of stiffness is observed when the viscosity is decreased, as shown in the remaining plots in Figs. 5(c) and (d) for the much lower viscosity of $\mu = 0.04$.

It is precisely the parameter regime corresponding to large fibre force and small viscosity where immersed boundary computations have been observed to encounter the most difficulty. In numerous heart valve simulations reported in the literature [16, 18], a careful scaling argument was required to justify choosing $\mu = 1.0$, instead of the actual viscosity of blood, $\mu \approx 0.04$, in order for the time step requirement in computations to be practical. The most significant conclusion that can be drawn from this discussion is that the stiffness in the immersed boundary method arises from the interaction of the fibre and fluid, through a combination of large fibre force and small viscosity, rather than the high Reynolds number effects that limit typical fluid flow calculations for other problems not characterised by this fluid–structure interaction.

A simple strategy for countering the stiffness is to search for different explicit schemes that deal more effectively with solution modes that tend to cluster near the imaginary axis. An obvious candidate for an alternative explicit time-stepping technique is the Runge–Kutta (RK) family of schemes. Figure 6 presents the results of fully explicit computations using

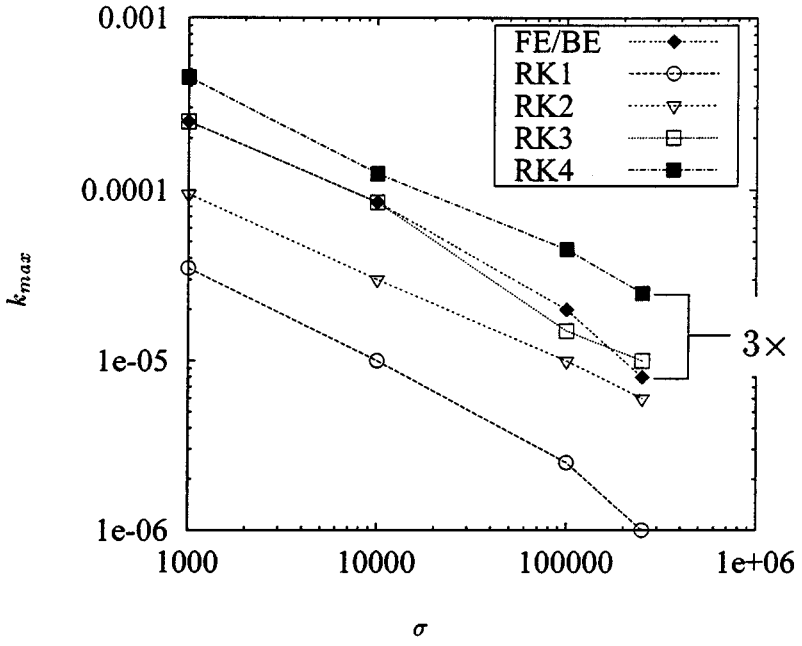

FIG. 6. Comparison of computed time step restrictions for the Runge–Kutta schemes and the ADI implementation of the immersed boundary method, for $\mu = 0.01$.

TABLE II
CPU Times for the $\sigma = 2.5 \times 10^5$ Full Immersed Boundary Computations in Fig. 6

	CPU time required[b]	
Scheme	$\mu = 1.0$	$\mu = 0.01$
*RK*1	370.59	1658.21
*RK*2	138.12	143.02
*RK*3	110.87	99.44
*RK*4	109.76	52.64
FE/BE	53.96	54.12

[a] Performed on an SGI Origin 2000 (4×195 MHz R10000 processors, 512 Mb RAM).
[b] In seconds.

the Runge–Kutta schemes of orders 1 through 4, for various choices of the fibre forcing parameter. The semi-implicit *FE/BE* results are included for comparison. We can see from the plots of maximum time step for the various RK schemes (along with the accompanying CPU times in Table II) that the *RK*4 scheme is the best of all the explicit methods considered, and becomes comparable in cost to the *FE/BE* method, particularly when the viscosity is reduced. While the semi-implicit approach is very similar in principle to the *RK*1 method, there is clearly a great deal of advantage to be gained from its implicit treatment of the diffusion term, about which more will be said in the next section.

4.2. *Stability of the FE/BE Scheme*

We begin by rewriting the equations of motion and identifying the terms that are discretised implicitly and explicitly:

$$\frac{\partial \mathbf{u}}{\partial t} = \underbrace{\frac{1}{\rho}\bar{\mathcal{S}}\sigma\frac{\partial^2 \mathbf{X}}{\partial s^2}}_{\text{explicit}} + \underbrace{\frac{\mu}{\rho}\Delta\mathbf{u} - \frac{1}{\rho}\nabla p}_{\text{implicit}}, \tag{19}$$

$$\nabla \cdot \mathbf{u} = 0, \tag{20}$$

$$\frac{\partial \mathbf{X}}{\partial t} = \underbrace{\mathcal{S}\mathbf{u}}_{\text{explicit}}. \tag{21}$$

The symbols $\mathcal{S}$ and $\bar{\mathcal{S}}$ represent the delta function interpolation operators, which transfer between grid quantities $\mathbf{V}(\mathbf{x})$ and fibre grid quantities $\mathbf{W}(s)$ as follows:

$$\mathcal{S}\mathbf{V}(\mathbf{x}) = \int_\Omega \mathbf{V}(\mathbf{x}) \cdot \delta_\epsilon(\mathbf{x} - \mathbf{X}(s,t))\, d\mathbf{x} \qquad \text{and} \qquad \bar{\mathcal{S}}\mathbf{W}(s) = \int_\Gamma \mathbf{W}(s) \cdot \delta_\epsilon(\mathbf{x} - \mathbf{X}(s,t))\, ds.$$

If we discretise these equations in time only, using the *FE/BE* scheme described in Section 2.2, then we have

$$\mathbf{u}^n - \frac{k\mu}{\rho}\Delta\mathbf{u}^n + \frac{k}{\rho}\nabla p^n = \mathbf{u}^{n-1} + \frac{k}{\rho}\bar{\mathcal{S}}\sigma\frac{d^2}{ds^2}\mathbf{X}^{n-1}, \tag{22}$$

$$\nabla \cdot \mathbf{u}^n = 0, \tag{23}$$

$$\mathbf{X}^n = \mathbf{X}^{n-1} + k\mathcal{S}\mathbf{u}^n, \tag{24}$$

where we have abused notation somewhat by denoting semi-discrete quantities at time t_n (which are continuous in space only) by a superscript $(\cdot)^n$.

We now investigate the time stability of solutions to Eqs. (22)–(24) by assuming that $\mathbf{u}^n$ and $\mathbf{X}^n$ depend on the solutions at the previous time step as

$$\mathbf{u}^n = \gamma \mathbf{u}^{n-1} \qquad \text{and} \qquad \mathbf{X}^n = \gamma \mathbf{X}^{n-1},$$

where the *amplification factor* γ replaces $e^{\lambda t}$ from the time-continuous analysis. Once again, we look for separable solutions of the form

$$\begin{Bmatrix} \mathbf{u} \\ p \end{Bmatrix}^n = e^{\hat{\imath}\alpha x} \begin{Bmatrix} \hat{\mathbf{u}}(y) \\ \hat{p}(y) \end{Bmatrix}^n \qquad \text{and} \qquad \mathbf{X}^n = e^{\hat{\imath}\alpha\theta s}\hat{\mathbf{X}}^n,$$

which on substitution into the time-discrete equations yields a system of ODEs for the solution components as functions of y. It should be clear to the reader that the solution process closely parallels that described in Section 3.2, and so we omit the details of the derivation. At the end, we obtain a dispersion relation which gives the amplification factor in terms of the other parameters in the problem. The *FE/BE* scheme is stable provided that all γ arising from this equation satisfy $|\gamma| < 1$.

As before, we apply a Newton iteration, with continuation in the smoothing radius ϵ, to solve the dispersion relation over a range of time steps and for all wavenumbers $\alpha/2\pi \in [1, 64]$. The character of the amplification factors is exactly what we would expect given our previous experience with the modal analysis of the continuous problem. We find that for time steps below a certain critical value, $k < k_{\max}$, all roots satisfy $\gamma < 1$ and the first to become unstable for $k > k_{\max}$ corresponds to a tangential mode of oscillation in the fibre. The critical time step $k_{\max}$ is given in Table III for various forcing parameters, with the corresponding time step limit observed in computations with the same fibre force. In all cases, our analysis predicts a $k_{\max}$ which is consistently one-half as large as the actual time step limit encountered in computations. Considering the approximations that have been made in our idealised discretisation, this discrepancy is not surprising.

4.3. *Semi-implicit, Iterative Schemes*

Instead of solving Eqs. (22)–(24) in an explicit, two-step process, the iterative scheme in [13] couples the fibre evolution equation implicitly with the solution of the fluid equations.

TABLE III

A Comparison of the Maximum Time Step Predicted by the Theory and Observed in Computations for the *FE/BE* Method, with $N = 64$, $\epsilon = \frac{1}{64}$, $\mu = 1$

σ	$k_{\max}$ (theory)	$k_{\max}$ (computed)
10^2	4×10^{-3}	8×10^{-3}
10^3	2×10^{-4}	6×10^{-4}
10^4	6×10^{-5}	1×10^{-4}
10^5	8×10^{-6}	2×10^{-5}

In essence, this involves replacing quantities $(\cdot)^n$ at time level n with values $(\cdot)^{n,m}$, where m refers to the iteration number. The coupling comes from replacing $\mathbf{X}^{n-1}$ in Eq. (22) with $\mathbf{X}^{n,m-1}$. We make a change of notation here, and write the Stokes solve represented by Eqs. (22) and (23) symbolically, using the operator $\mathcal{H}$ as

$$\mathbf{u}^{n,m} = \mathcal{H}\left(\mathbf{u}^{n-1} + \frac{k}{\rho}\bar{\mathcal{S}}\sigma\frac{d^2}{ds^2}\mathbf{X}^{n,m-1}\right),$$
$$\mathbf{X}^{n,m} = \mathbf{X}^{n-1} + k\mathcal{S}\mathbf{u}^{n,m}.$$

By substituting the expression for $\mathbf{u}^{n,m}$ into the fibre evolution equation, the iteration may be written as a single equation for $\mathbf{X}$,

$$\mathbf{X}^{n,m} = \underbrace{\mathbf{X}^{n-1} + k\mathcal{S}\mathcal{H}\mathbf{u}^{n-1}}_{\mathbf{Z}^{n-1}} + \mathcal{S}\mathcal{H}\bar{\mathcal{S}}\underbrace{\frac{\sigma k^2}{\rho}\frac{d^2}{ds^2}}_{\mathcal{A}}\mathbf{X}^{n,m-1},$$

or more compactly as

$$\mathbf{X}^{n,m} = \mathbf{Z}^{n-1} + \mathcal{S}\mathcal{H}\bar{\mathcal{S}}\mathcal{A}\mathbf{X}^{n,m-1}. \tag{25}$$

In practice, this iteration converges very slowly, and the convergence is speeded considerably by using the modified iteration

$$(\mathcal{I} - \mathcal{D}\mathcal{A})\,(\mathbf{X}^{n,m} - \mathbf{X}^{n,m-1}) = \mathbf{Z}^{n-1} - (\mathcal{I} - \mathcal{S}\mathcal{H}\bar{\mathcal{S}}\mathcal{A})\mathbf{X}^{n,m-1}, \tag{26}$$

which clearly has the same solution as (25). Here, $\mathcal{I}$ signifies the identity operator, and $\mathcal{D} = \mathcal{S}\bar{\mathcal{S}}$ is a scaling factor. In the fully discrete setting, $(\mathcal{I} - \mathcal{S}\mathcal{H}\bar{\mathcal{S}}\mathcal{A})$ is a dense matrix, while $(\mathcal{I} - \mathcal{D}\mathcal{A})$ is a block tridiagonal preconditioner which accelerates convergence.

To quantify the rate of convergence, we again look for solutions of the form $\mathbf{X}^{n,m} = e^{i\alpha x}\hat{\mathbf{X}}^{n,m}$ on each of the subdomains $\Omega_0^{\pm}$ and Ω_0^{ϵ}, and solve the resulting system of ODEs as before. While the solution procedure is very similar to that seen above, it is important to realise that there is one very significant difference from the continuous problem: rather than define the fluid force implicitly in terms of the fibre position, we compute the force *on the basis of the fibre position from the previous iteration*. Consequently, the semi–discrete analogue of the fibre iteration (26) is an explicit formula for $\hat{\mathbf{X}}^{n,m}$ in terms of $\hat{\mathbf{X}}^{n,m-1}$, and so our analytical solution procedure is simplified considerably.

Equation (26) reduces to an iteration of the form

$$\mathcal{B}\hat{\mathbf{X}}^{n,m} = \mathcal{C}\hat{\mathbf{X}}^{n,m-1} + \mathbf{R}^{n-1},$$

where $\mathcal{B}$ and $\mathcal{C}$ are 2×2 matrices, and $\mathbf{R}^{n-1}$ is a 2-vector with entries evaluated at the previous time step. Since we are only interested in the rate of convergence of the iteration, it is expedient for us to consider the difference between successive iterates

$$\mathbf{E}^{n,m} = \hat{\mathbf{X}}^{n,m} - \hat{\mathbf{X}}^{n,m-1},$$

which satisfies the recurrence relation

$$\mathbf{E}^{n,m} = \mathcal{M}\mathbf{E}^{n,m-1},$$

where $\mathcal{M} = \mathcal{B}^{-1}\mathcal{C}$ is the *iteration matrix*. The convergence properties of the iteration are manifested in the eigenvalues of $\mathcal{M}$, which can be found using MAPLE as

$$\varrho_t = \frac{\sigma_t \pi^4 k^2 \sin^2(\alpha\epsilon)(-\pi^4 + \pi^4 e^{-2\alpha\epsilon} + 5\pi^2\alpha^3\epsilon^3 + 3\alpha^5\epsilon^5 + 2\pi^4\alpha\epsilon)}{\alpha\epsilon(\alpha^2\epsilon^2 + \pi^2)^2\left(-4\alpha^4\epsilon^7 + 8\alpha^2\epsilon^5\pi^2 - 4\epsilon^3\pi^4 + 3\sigma_t\pi^4 k^2 \sin^2(\alpha\epsilon)\right)}, \quad (27)$$

$$\varrho_n = \frac{\sigma_n \pi^6 k^2 \sin^2(\alpha\epsilon)(\pi^2 - \pi^2 e^{-2\alpha\epsilon} + \alpha^3\epsilon^3 + \pi^2\alpha\epsilon)}{\alpha\epsilon(\alpha^2\epsilon^2 + \pi^2)^2\left(-4\alpha^4\epsilon^7 + 8\alpha^2\epsilon^5\pi^2 - 4\epsilon^3\pi^4 + 3\sigma_n\pi^4 k^2 \sin^2(\alpha\epsilon)\right)}. \quad (28)$$

Just as the solution to the continuous problem exhibited a decoupling between normal and tangential modes, so also does the convergence of the semi-discrete scheme depend on two distinct eigenvalues, corresponding to normal and tangential forcing. The convergence of the scheme is governed by $\varrho_{\max} = \max(|\varrho_t|, |\varrho_n|)$: if $\varrho_{\max} < 1$, the iteration converges; otherwise it diverges. A contour plot of $\varrho_{\max}$ is given in Fig. 7, for parameter values $\mu = 1$ and $\sigma = 10^4$. We observe that the iteration always converges, which is to be expected, since the scheme was proven to be unconditionally convergent in [13]. Furthermore, for a given time step the slowest mode to converge is the tangential mode; therefore, just as tangential modes provide the greatest contribution to the stiffness in the problem, so also do they govern the convergence of the *MP* iteration.

We also performed numerical experiments on the same "flat fibre" model problem used in Section 3.3 in order to verify the predicted convergence rates, and the results are summarised

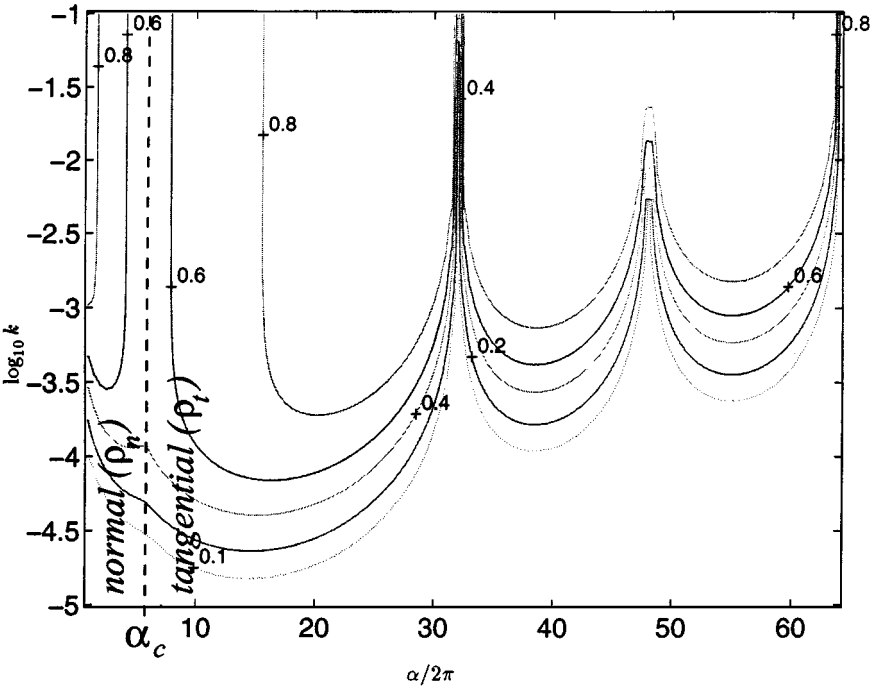

FIG. 7. Convergence rate contours for the *MP* scheme. The vertical dotted line separates the parameter space into regions where the convergence rate for the normal mode (left) or the tangential mode (right) is largest ($\sigma = 10^4$).

TABLE IV
Convergence Rates Predicted by Theory and Observed in Full Immersed Boundary Computations for the *MP* Iterative Scheme

	$\sigma = 10^3$		$\sigma = 10^4$		$\sigma = 10^5$	
k	Theor.	Comp.	Theor.	Comp.	Theor.	Comp.
0.0001	0.01	0.01	0.08	0.08	0.43	0.43
0.0025	0.05	0.05	0.33	0.33	0.75	0.76
0.0005	0.17	0.18	0.62	0.62	0.84	—
0.0010	0.43	0.43	0.79	0.79	0.87	—
0.0025	0.75	0.73	0.86	—	0.88	—
0.0050	0.84	0.84	0.88	—	0.88	—

Note. The "—" entries correspond to instances where the scheme became unstable.

in Table IV. Convergence rates were computed from numerical results using the formula

$$\text{Rate} = \frac{\text{Res}^{m+1}}{\text{Res}^m},$$

where

$$\text{Res}^m = \left[\frac{1}{N_b} \sum_{l=0}^{N_b-1} \left\| \mathbf{X}_l^m - \mathbf{X}_l^{m-1} \right\|_2^2 \right]^{1/2}$$

is the residual at iteration level m and $\|\cdot\|_2$ is the standard L_2–norm on vectors. The predicted convergence rates were found by reading off $\varrho_{\max}$ for the dominant ($\alpha = 2\pi$) mode on the contour plot in Fig. 7, which always correspond to the normal fibre modes. Even though the tangential convergence rate is invariably the largest for the entire range of α in any given computation, and hence should dominate the convergence after a large number of iterations, they are also the modes whose amplitudes decay much more rapidly in time. Within every time step, only ten or so iterations were typically required to satisfy the residual tolerance, and so it is to be expected that the lowest wavenumber, normal modes will dominate the actual convergence rate observed in computations.

The blank entries in the table correspond to instances where the computation was unstable, which seems to go against our analytical predictions of unconditional convergence. However, we believe that this arises from a time instability which affects the numerical scheme when the time step is taken too large. In fact, the results in [13, p. 269] show that even though the scheme is convergent and *more* stable in time than the fully explicit method, it is not *always* stable. While our analysis captures the convergence rate quite well, it is unable to predict onset of instability in computations.

4.4. *Comparison*

Before closing our discussion of time discretisations, we will draw a comparison between the explicit and semi-implicit approaches just described. We consider another test problem more typical of that seen in the literature [11, 13, 15], in which the fibre is a closed loop which initially has the shape of an ellipse. As shown in Fig. 8, the semi–axes of the

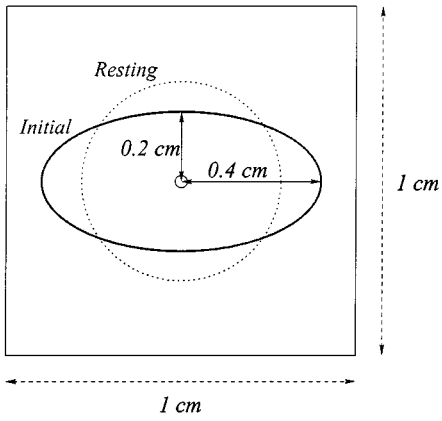

FIG. 8. The "ellipse" test problem: the initial fibre position is an ellipse with semi-axes 0.4 and 0.2 cm. The equilibrium state is a circle with radius approximately 0.2828 cm.

ellipse are of lengths 0.2 and 0.4 cm, and we use the same linear force density function with stiffness constant σ. The ellipse will tend toward an equilibrium state that is a circle with the same area as that of the original ellipse (and radius of approximately 0.2828 cm) because the fluid is incompressible. The reason for choosing this problem rather than the sinusoidally perturbed flat fibre is that the area (or "volume") of fluid inside the ellipse can be used as a measure of the numerical error. Immersed boundary computations are known to experience loss of volume, which becomes significant during more extreme flow conditions such as those we are considering here with large σ. This volume loss problem was identified in [18] and shown to arise not from fluid passing physically through the immersed boundary, since the fibre points move along streamlines, but rather from the fact that the interpolated velocity field through which the immersed boundary moves is not discretely divergence-free. LeVeque and Li showed in [11] that the volume loss in the immersed boundary method for a problem nearly identical to our ellipse example grows linearly in time. A modification of the divergence stencil was developed in [18] which reduces the volume loss significantly (at the expense of an increase in the cost of delta function interpolation). We have not implemented this modified stencil in our simulations.

We applied the *RK*1, *RK*4, *FE*/*BE*, and *MP* methods to this problem and list in Table V the maximum time steps and CPU times required for each method for two sets of computations with $\sigma = 10^4$ and 10^5. Among the fully explicit schemes, the *RK*4 method is up to an order of magnitude more efficient than Forward Euler (or *RK*1). We also see that *RK*4 is competitive, in terms of CPU time, with the *FE*/*BE* method.

Moving to the *MP* scheme, we saw in Table IV that coupling the fibre and fluid together within an iteration does allow a time step much larger than that for explicit schemes to be taken. However, there is a corresponding increase in the rate of volume loss, which is given in Table V as a change in area relative to the initial 0.251 cm^2. We chose two representative time steps for the *MP* scheme in Table V, from which it is clear that while stability restrictions are much more lenient than those for the other schemes, the method suffers from a much more severe loss of volume if k is taken too large. In fact, there is no advantage to using the iterative scheme if we require a level of volume loss comparable to that experienced by the other schemes.

TABLE V
Comparison of Computational Costs for Several Explicit and Semi-implicit Schemes with $N = 64$ and $N_b = 192$

	$\sigma = 10^4,\ t_{\text{end}} = 0.020$			$\sigma = 10^5,\ t_{\text{end}} = 0.005$		
Scheme	$k_{\max}$	% Vol. loss	CPU[a]	$k_{\max}$	% Vol. loss	CPU[a]
*RK*1	1.3×10^{-5}	2.8	114.31	1.0×10^{-6}	4.4	372.49
*RK*4	8.0×10^{-5}	2.4	66.51	3.0×10^{-5}	4.4	44.16
FE/*BE*	7.0×10^{-5}	4.4	28.45	1.0×10^{-5}	5.2	49.00
MP	8.0×10^{-5}	8.4	56.62	2.5×10^{-5}	6.8	44.00
	1.6×10^{-4}	13.1	29.99	5.0×10^{-5}	11.9	26.72

Note. The time step $k_{\max}$ was chosen to be the largest allowed by the method for stability, except for the *MP* scheme (which always converged). The "volume loss" is computed relative to the equilibrium value of 0.251 cm^2. CPU timings were taken on an SGI Origin 2000 (4×195 MHz R10000 processors, 512 Mb RAM).

[a] In seconds.

We can conclude from these results that while the *MP* iteration may be unconditionally convergent and allow significantly larger time steps to be taken, the time step is still limited by the accumulation of error in the incompressibility condition. Clearly, there is a need for more work to be done on developing new time-stepping strategies to treat the force implicitly in some type of iteration, while at the same time controlling the volume error.

Our observation that an appropriately chosen explicit discretisation performs as well as or better than any of the implicit methods used in practice, particularly when the fibre force is large, should prove to be very helpful in improving the performance of the immersed boundary method. Since the *FE*/*BE* method handles the fibre terms in the equations with a Forward Euler step, it seems reasonable to suppose that we can take advantage of the particular nature of the fibre modes by combining a Runge–Kutta discretisation for the fibre along with implicit handling of the remaining terms in the equations. A class of schemes that fits these requirements exactly is the Implicit–Explicit Runge–Kutta (or *IMEX–RK*) family introduced in [1]. These methods have the additional advantage that they require minimal changes to the existing logic in the immersed boundary code. We applied several *IMEX–RK* methods of various orders to the immersed fibre problem, and found that the performance was comparable to the *RK*4 and *FE/BE* results, with the latter differing from the first order *FE* or *RK*1 method only in its implicit treatment of diffusion. While this outcome is somewhat disappointing, our straightforward implementation clearly leaves room for further investigation. We expect that more sophisticated approaches may lead to significant improvements, which may become more evident in Navier–Stokes computations with high Reynolds number, convection-dominated flows.

5. SUMMARY AND CONCLUSIONS

In this paper, we have investigated the immersed fibre problem with a smoothed delta-function force. By restricting wavenumbers to a fixed range $[1, N]$ we were able to investigate "idealised discretisations" which neglected discrete grid effects. Our analysis was able to predict observed time step restrictions for several explicit and semi-implicit time-stepping methods. Our theoretical results suggested that the explicit time-stepping scheme *RK*4 would be appropriate for this problem and we demonstrate that *RK*4 can give a

performance comparable to that of the standard *FE*/*BE* scheme for extreme conditions, such as those arising from large fibre forcing and small viscosity. We observed that the stiffest modes arise from the class of tangential fibre oscillations. It is possible that some type of preconditioning strategy based on this special property of the solution, perhaps by performing a local linearisation that decouples the normal and tangential motions of the fibre, may lead to more efficient iterative schemes. A similar technique was used in [9] for removing the stiffness in interfacial flows governed by surface tension effects. This will be the subject of future work.

APPENDIX: DISPERSION RELATION

The dispersion relation summarised in Eq. [18] as $S_n^\epsilon(\beta) \cdot S_t^\epsilon(\beta) = 0$ has two factors that can be obtained with the aid of MAPLE:

$$\begin{aligned}
S_n^\epsilon(\beta) &= -4\epsilon^2\beta^3(\alpha^2\epsilon^2+\pi^2)^2(\beta^2\epsilon^2+\pi^2)^2(\alpha^2-\beta^2)^2 \\
&\quad + \frac{\sigma_n\rho^2\hat{D}_\epsilon^{\,2}}{\mu^2}[\pi^4\alpha\beta^3(\beta^2\epsilon^2+\pi^2)^2(1-e^{-2\alpha\epsilon}) - \pi^4\alpha^4(\alpha^2\epsilon^2+\pi^2)^2(1-e^{-2\beta\epsilon}) \\
&\quad + \epsilon\alpha^2\beta(\alpha^2\epsilon^2+\pi^2)(\beta^2\epsilon^2+\pi^2)(\alpha^2-\beta^2)(3\epsilon^4\alpha^2\beta^2+2\epsilon^2\pi^2(\alpha^2+\beta^2)+2\pi^4)], \\
S_t^\epsilon(\beta) &= 4\epsilon^2\beta(\alpha^2\epsilon^2+\pi^2)^2(\beta^2\epsilon^2+\pi^2)^2(\alpha^2-\beta^2)^2 \\
&\quad + \frac{\sigma_t\rho^2\hat{D}_\epsilon^{\,2}}{\mu^2}[\pi^4\alpha\beta(\beta^2\epsilon^2+\pi^2)^2(1-e^{-2\alpha\epsilon}) - \pi^4\alpha^2(\alpha^2\epsilon^2+\pi^2)^2(1-e^{-2\beta\epsilon}) \\
&\quad - \epsilon^3\alpha^2\beta\pi^2(\alpha^2\epsilon^2+\pi^2)(\beta^2\epsilon^2+\pi^2)(\alpha^2-\beta^2)].
\end{aligned}$$

An asymptotic expansion of both factors (see [21] for details) for small values of the smoothing radius ϵ indicates that

$$\begin{aligned}
S_n^\epsilon(\beta) &= S_n^0(\beta) + \epsilon S_n^0(\beta) + \mathcal{O}(\epsilon^2), \\
S_t^\epsilon(\beta) &= S_t^0(\beta) + \mathcal{O}(\epsilon),
\end{aligned}$$

where $S_n^0(\beta)$ and $S_t^0(\beta)$ are the dispersion relations from the "jump problem" with $\epsilon = 0$, given in [23]. Therefore, the modes for the smoothed delta function problem reduce to those of the jump formulation as $\epsilon \to 0$.

ACKNOWLEDGMENTS

The work of J. M. Stockie was supported in part by a Post Graduate Scholarship from the Natural Sciences and Engineering Research Council of Canada (while at the University of British Columbia) and a Postdoctoral Fellowship from the Pacific Institute for the Mathematical Sciences. The work of B. R. Wetton was supported by an NSERC Research Grant. The authors thank Dr. Michael Monagan, whose helpful suggestions allowed us to complete the MAPLE determinant calculations.

REFERENCES

1. U. M. Ascher, S. J. Ruuth, and R. J. Spiteri, Implicit–explicit Runge–Kutta methods for time–dependent partial differential equations, *Appl. Numer. Math.* (Special Issue on Innovative Time Integrators) **25**(2/3), 151 (1997).
2. R. P. Beyer and R. J. LeVeque, Analysis of a one-dimensional model for the immersed boundary method, *SIAM J. Numer. Anal.* **29**(2), 332 (1992).

3. Y. C. Chang, T. Y. Hou, B. Merriman, and S. Osher, A level set formulation of Eulerian interface capturing methods for incompressible fluid flows, *J. Comput. Phys.* **124**, 449 (1996).
4. B. W. Char *et al.*, *Maple V Language Reference Manual* (Springer-Verlag, Berlin/New York, 1991).
5. R. Cortez and D. A. Varela, The dynamics of an elastic membrane using the impulse method, *J. Comput. Phys.* **138**, 224 (1997).
6. L. J. Fauci and C. S. Peskin, A computational model of aquatic animal locomotion, *J. Comput. Phys.* **77**, 85 (1988).
7. A. L. Fogelson, Continuum models of platelet aggregation: Formulation and mechanical properties, *SIAM J. Appl. Math.* **52**(4), 1089 (1992).
8. A. L. Fogelson and C. S. Peskin, A fast numerical method for solving the three-dimensional Stokes' equations in the presence of suspended particles, *J. Comput. Phys.* **79**, 50 (1988).
9. T. Y. Hou, J. S. Lowengrub, and M. J. Shelley, Removing the stiffness from interfacial flows with surface tension, *J. Comput. Phys.* **114**, 312 (1994).
10. G. Lapenta, F. Iinoya, and J. U. Brackbill, Particle-in-cell simulation of glow discharges in complex geometries, *IEEE Trans. Plasma Sci.* **23**(4), 769 (1995).
11. R. J. LeVeque and Z. Li, Immersed interface methods for Stokes flow with elastic boundaries or surface tension, *SIAM J. Sci. Comput.* **18**(3), 709 (1997).
12. R. J. LeVeque, C. S. Peskin, and P. D. Lax, Solution of a two-dimensional cochlea model with fluid viscosity, *SIAM J. Appl. Math.* **48**(1), 191 (1988).
13. A. A. Mayo and C. S. Peskin, An implicit numerical method for fluid dynamics problems with immersed elastic boundaries, in *Fluid Dynamics in Biology: Proceedings, AMS–IMS–SIAM Joint Summer Research Conference on Biofluiddynamics*, edited by A. Y. Cheer and C. P. van Dam, Contemporary Mathematics (Am. Math. Soc. Providence, RI, 1993), Vol. 141, pp. 261–277.
14. D. M. McQueen and C. S. Peskin, Shared-memory parallel vector implementation of the immersed boundary method for the computation of blood flow in the beating mammalian heart, *J. Supercomputing* **11**, 213 (1997).
15. C. S. Peskin, Numerical analysis of blood flow in the heart, *J. Comput. Phys.* **25**, 220 (1977).
16. C. S. Peskin and D. M. McQueen, A three-dimensional computational model for blood flow in the heart. I. Immersed elastic fibers in a viscous incompressible fluid, *J. Comput. Phys.* **81**, 372 (1989).
17. C. S. Peskin and D. M. McQueen, A general method for the computer simulation of biological systems interacting with fluids, in *Biological Fluid Dynamics*, edited by C. P. Ellington and T. J. Pedley, Symposia of the Society for Experimental Biology (Soc. Exper. Biol., Leeds, 1995), Vol. 49, pp. 265–276.
18. C. S. Peskin and B. F. Printz, Improved volume conservation in the computation of flows with immersed elastic boundaries, *J. Comput. Phys.* **105**, 33 (1993).
19. A. M. Roma, *A Multilevel Self Adaptive Version of the Immersed Boundary Method*, Ph.D. thesis, New York University (1996).
20. M. E. Rosar, *A Three Dimensional Model for Fluid Flow through a Collapsible Tube*, Ph.D. thesis, New York University (1994).
21. J. M. Stockie, *Analysis and Computation of Immersed Boundaries, with Application to Pulp Fibres*, Ph.D. thesis, Institute of Applied Mathematics, University of British Columbia, Vancouver, BC, Canada (1997). Available at `http://www.math.sfu.ca/~jms/`. [unpublished]
22. J. M. Stockie and S. I. Green, Simulating the motion of pulp fibres using the immersed boundary method, *J. Comput. Phys.* **147**(1), 147 (1998).
23. J. M. Stockie and B. T. R. Wetton, Stability analysis for the immersed fiber problem, *SIAM J. Appl. Math.* **55**(6), 1577 (1995).
24. A.-K. Tornberg, R. W. Metcalfe, L. R. Scott, and B. Bagheri, A front-tracking method for simulating fluid particle motion using high-order finite element methods, in *Proceedings, 1997 ASME Fluids Engineering Division Summer Meeting, Vancouver, Canada, June 22–26, 1997*.
25. C. Tu and C. S. Peskin, Stability and instability in the computation of flows with moving immersed boundaries: A comparison of three methods, *SIAM J. Sci. Statist. Comput.* **13**(6), 1361 (1992).
26. S. O. Unverdi and G. Tryggvason, A front-tracking method for viscous, incompressible, multi-fluid flows, *J. Comput. Phys.* **100**, 25 (1992).